J. Electrochem. Sci. Eng. **9(4)** (2019) 255-267; http://dx.doi.org/10.5599/jese.634

Open Access: ISSN 1847-9286
https://pub.iapchem.org/ojs/index.php/JESE

Original scientific paper

Synthesis and characterization of $LaMnO_3$ nanocrystals and graphene oxide: fabrication of graphene oxide–$LaMnO_3$ sensor for simultaneous electrochemical determination of hydroquinone and catechol

Sedighe Akbari[1], Mohammad Mehdi Foroughi[1,✉], Hadi Hassani Nadiki[1] and Shohreh Jahani[2]

[1]*Department Department of Chemistry, Kerman Branch, Islamic Azad University, Kerman, Iran*
[2]*NanoBioElectrochemistry Research Center, Bam University of Medical Sciences, Bam, Iran*

Corresponding author: ✉mohammadmehdi869@yahoo.com; Tel. +98 34331321750

Received: November 1, 2018; Revised: April 7, 2019; Accepted: May 9, 2019

Abstract

For the first time, a new method for preparation of graphene oxide-$LaMnO_3$ (GO-$LaMnO_3$) nanocomposite as a material of electrochemical sensor for simultaneous determination of catechol (CT) and hydroquinone (HQ) is developed. $LaMnO_3$ nanoparticles have been characterized by Fourier-transform infrared spectroscopy (FT-IR), scanning electron microscopy (SEM), X-ray diffraction (XRD), transmission electron microscopy (TEM) and energy dispersive X-ray analysis (EDX) technique. Due to the excellent catalytic activity, enhanced electrical conductivity and high surface area, the simultaneous determination of HQ and CT with two well-defined peaks has been achieved at the GO-$LaMnO_3$ modified electrode. Comparing with unmodified electrodes, the oxidation currents of HQ and CT increased remarkably. Also, the result exhibited a great decrease in anodic overpotential resulting in about 150 mV negative shift of potential. The catalytic peak current values are found linearly dependent on the HQ and CT concentrations in the range of 0.5–433.3 and 0.5–460.0 μM with sensitivity of 0.0719 and 0.0712 μA μM^{-1}, respectively. The detection limits for HQ and CT are determined as 0.06 and 0.05 μM, respectively.

Keywords

Catechol; hydroquinone; graphene oxide; $LaMnO_3$ nanoparticles; voltammetry

Introduction

Phenolic materials compounds are widely used in a broad class of industries, such as coal mining, cosmetics, paint, pharmaceutical preparation and polymer [1]. During the manufacturing and application process of these compounds, some of them are unintentionally released into environment,

polluting thus ground waters and rivers. Catechol (CT) and hydroquinone (HQ) are two most important isomers of phenolic materials which are announced as environmental contaminants by the European Union and the US Environmental Protection Agency [2]. Simultaneous determination of HQ and CT is very important for environmental analysis because they coexist in environmental samples as environmental contaminants of high toxicity and too difficult to degrade [3]. CT has also been found in cigarette smoke and researches have demonstrated that it induces damage to DNA and can cause cancer [4,5]. Hence, it is essential to develop a sensitive, simple, rapid and cheap analytical method for determination of dihydroxybenzene isomers. So far, many analytical methods have been reported for their determination, such as capillary zone electrophoresis, liquid chromatography, synchronous fluorescence, gas chromatography/mass spectrometry, chemiluminescence, and pH based-flow injection analysis [6-12]. Electrochemical methods have some attractive advantages such as simple and fast response, low maintenance cost, excellent selectivity and high sensitivity. However, a serious obstacle is that the oxidation peak potentials of the isomers are too close at a bare electrode which causes overlapping of voltammetric responses, making their discrimination very difficult [13-17]. A chemically modified electrode is a superior approach to solve the peak separation problem by applying a modifier [18-24]. Hence, a few modified electrodes have already been reported to determine HQ and CT such as GCE modified by carbon nanotubes (CNT), poly-amid sulfonic acid-CNTs, graphene–chitosan composite, carbon nanotubes/poly (3-methylthiophene), penicillamine), Zn/Al layered double hydroxide film, or gold-graphene [25-31].

Graphene (Gr) nano sheets have a great potential for the applications in the development of electrochemical sensors and biosensors. Gr is used as a support material to improve the electrochemical reactivity of molecules on the surface of modified electrode, what is due to its superior mechanical, electrical, thermal, and optical properties [32]. On the other side, its low energy storage capacity greatly hinders its extensive use. To overcome these shortcomings, many researches have been focused on the synthesis of graphene-based inorganic composites. Recently, the synthesis procedures of new composites of graphene with inorganic particles, such as metal, metal oxide, metal hydroxide, or metal sulfide particles, have been reported [33-38]. Due to presence of graphene and inorganic particles, the fabricated electrochemical sensors display exceptional improvement in electrical properties and functionality for different types of composites. Among inorganic particles, perovskite nanocrystals having electrically active structure and convenient magnetic and dielectric properties have been broadly studied and employed in the development of electrochemical gas sensors, solid fuel cells and many of electrochemical catalytic processes [39-44].

To the best of our knowledge, no study has already been reported for the electroanalysis and simultaneous determination of HQ and CT using GCE modified by GO-$LaMnO_3$. For the first time, we have described the preparation of a new, GO-$LaMnO_3$ modified GCE for the electroanalysis and determination of HQ and CT. In this paper, we have evaluated analytical performance of this sensor for simultaneous determination of HQ and CT by the voltammetry technique.

Experimental

Reagents and solutions

Manganese sulphate, lanthanum chloride and oleic acid were purchased from Merck and used as received. The HQ and CT were purchased from Sigma-Aldrich (Sigma-Aldrich, USA) and used as received. A 1.0×10^{-2} mol L^{-1} HQ and CT solution was prepared daily by dissolving appropriate amounts of HQ and CT in water and the solution was diluted to 100 mL with distilled deionized water. The solution was kept in a refrigerator in dark. More dilute solutions were prepared by serial dilution of

phosphate buffer solutions. Phosphate buffer solution (PBS, 0.1 mol L^{-1}) was prepared by mixing the stock solution of 0.1 mol L^{-1} NaH_2PO_4 and 0.1 mol L^{-1} Na_2HPO_4, and the pH was adjusted by HCl or NaOH. All other materials used were of analytical reagent grade and all solutions were prepared with double distilled deionized water. All chemicals were used without additional purification.

Apparatus

FT-IR spectra were recorded as KBr disks on a JASCO FT/IR-460 PLUS instrument. X-ray powder diffraction (XRD) analysis was conducted on a Philips analytical PC-APD X-ray diffractometer with graphite monochromatic Cu Kα radiation (α_1, λ_1 = 1.54056 Å, α_2, λ_2 = 1.54439 Å) to verify the formation of products. Surface analysis was done using a low vacuum JSM, 6380 LV scanning electron microscope (SEM) after coating the samples with a thin layer of gold by magnetron sputtering. Energy-dispersive X-ray spectrometry (EDX) is a significant nondestructive analytical tool typically applied for the chemical composition analysis. Electrochemical determinations were done with a SAMA 500 Electroanalyser (SAMA Research Center, Iran) controlled by a personal computer. The three-electrode electrochemical cell system consisted of glassy carbon working electrode (GCE, modified or unmodified), a saturated calomel reference electrode (SCE) and a Pt wire electrode as the auxiliary electrode. All electrochemical determinations were carried out under a pure nitrogen atmosphere at room temperature.

Synthesis of perovskite nanocrystal

In order to synthesize lanthanum manganese oxide nanocrystals, manganese sulphate and lanthanum chloride were chosen as starting materials. Solutions of manganese sulphate (10 ml, 0.1 M) and lanthanum chloride (10 ml, 0.1 M) were prepared and mixed together. Oleic acid (2 ml) was added into the pink solution. The pH of solution was adjusted to 7-8 by dropwise addition of NaOH (1.5 M) in the stirred solution. After complete precipitation, it was nebulized in the ultrasonic at 60 °C for 30 min. The precipitate was centrifuged for 15 min at (3000 rpm), washed with deionized distilled water and dried at 100 °C for 8 h. The achieved product was calcinated at 1100 °C for 6 h to let the sample self-ignite and burn off the impurity organic compound in the crystal.

Electrochemical synthesis of graphene oxide

The graphene oxide nano sheets were prepared by the electrochemical functionalization of graphite. In a typical synthesis, 10 mL 1-octyl-3-methyl-imidazolium hexafluorophosphate ($[C8mim]^+[PF_6]^-$) and 20 mL water were mixed and used as the electrolyte. A static potential of 2 V was applied between two graphite rods (6.0 cm distance between two rods) for 2 h and then potential increased to 6 V for 6 h. After corrosion for 6 h at room temperature, a black precipitate of GO was obtained at the bottom of the reactor. The black precipitate was separated and washed with ethanol and then sonicated for 30 min. The product was dried for 3 h in an oven at 70 °C.

Preparation of GCE and modified electrode

Prior to the surface modification, GCE was carefully polished with 0.3 µm and 0.05 µm alumina slurries to obtain a mirror-like surface. After sonication in water and ethanol successively for 20 s, the electrode was rinsed with water, and then dried under an infrared lamp. The GCE/GO-$LaMnO_3$ was prepared by casting 4 µL of GO-$LaMnO_3$ suspension (0.01 g $LaMnO_3$ + 0.005 g GO + 50 µL chitosan 1 % + 0.95 mL H_2O) on the surface of cleaned GCE. The solvent was then evaporated under an infrared heat lamp. As controls, GCE/GO and GCE/ $LaMnO_3$ were also fabricated with similar procedure by replacing GO-$LaMnO_3$ hybrid materials with GO or $LaMnO_3$, respectively.

Results and discussion

Characterization of $LaMnO_3$ nanocrystals

The FT-IR spectra of the pure oleic acid (a), precursor (b) and $LaMnO_3$ nanoparticles after calcination (c) are shown in Figure 1(A). In curve (a), two sharp bands at 2925 and 2854 cm^{-1} are attributed to the asymmetric CH_2 stretch and the symmetric CH_2 stretch, respectively. The intense peak at 1710 cm^{-1} was derived from the existence of the C=O stretch and the band at 1285 cm^{-1} exhibits the presence of the C–O stretch. In the curve (b), the asymmetric CH_2 stretch and the symmetric CH_2 are shifted to 2922 and 2853 cm^{-1}, respectively. The surfactant molecules in the adsorbed state were subjected to the field of the solid surface. As a result, the characteristic bands shifted to a lower frequency region which indicates that the hydrocarbon chains in the monolayer surrounding the precursor are in a closed-packed, crystalline state. All these bands disappeared when the precursor was calcinated at 800 °C, but two strong bands appear in the range of 400-600 cm^{-1} related to metal-O and O-metal-O vibration of $LaMnO_3$ perovskite (Fig. 1(A) (c)).

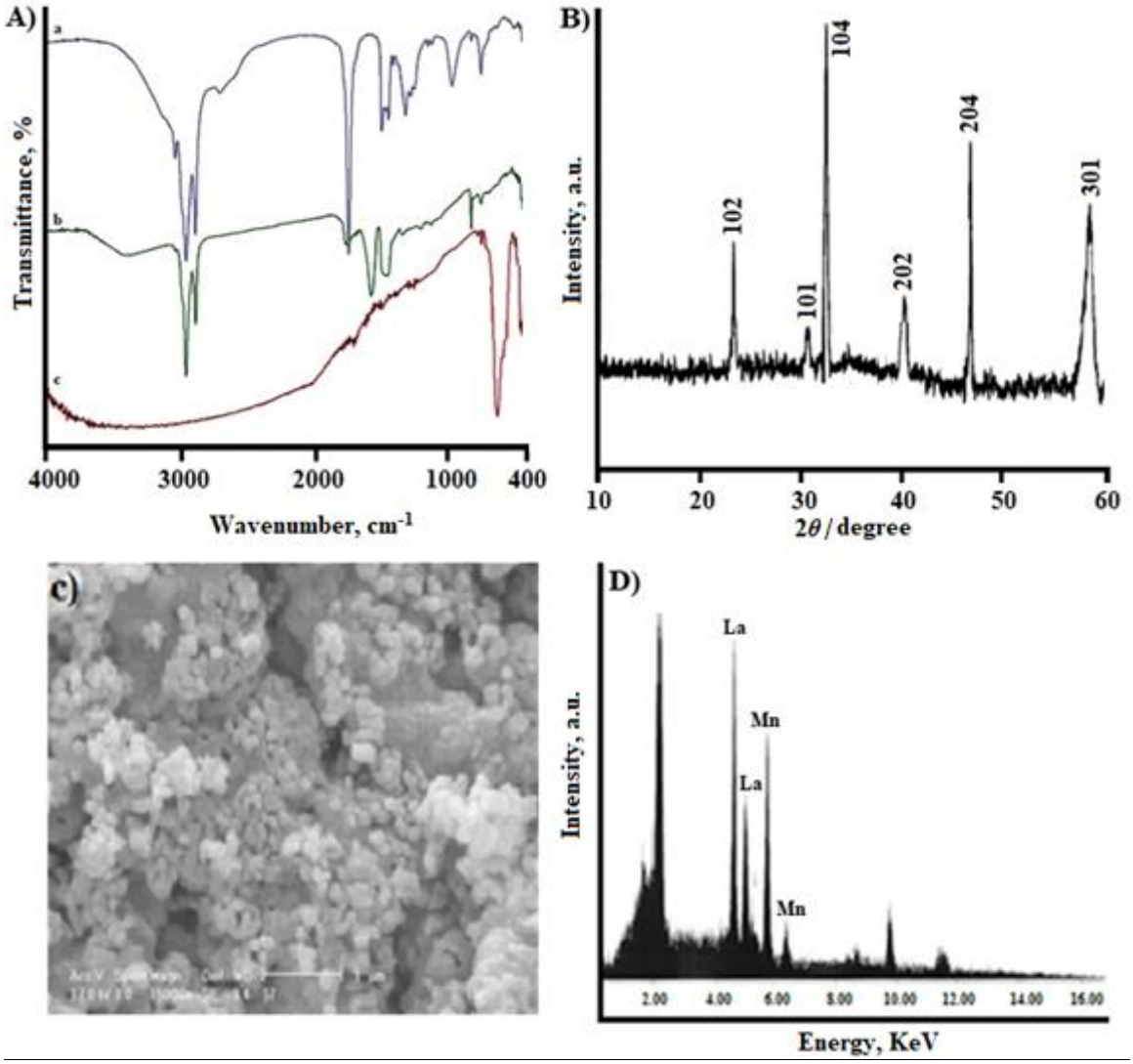

Figure 1. *(A) FT-IR spectra of (a) oleic acid, (b) precursor before calcination and (c) the product after calcination, (B) XRD pattern of the product, (C) SEM image of $LaMnO_3$ (D) EDX of nanocrystals*

XRD pattern of $LaMnO_3$ sample prepared *via* the ultrasonic-assisted co-precipitation process at 1100 °C is shown in Figure 1(B). For $LaMnO_3$ nanoparticles all diffraction peaks can be directly

indexed to a hexagonal phase of $LaMnO_3$ according to the JCPDS No. 23-0484 and no additional peaks for other impurities can be detected, indicating high purity of prepared sample. Furthermore, the narrow sharp peaks suggest that $LaMnO_3$ nanoparticles are well crystallized. The size distribution of $LaMnO_3$ nanoparticles has been estimated from the XRD spectra using the Debye–Scherrer equation [45]:

$$D_c = \frac{K\lambda}{\beta \cos\theta}$$

where *D* is the crystallite size, *K* is the so-called shape factor which usually takes a value about 0.9, λ is the wavelength of radiation, β is the corrected full width at half maximum (FWHM), and θ is diffraction angle. The crystallite size of $LaMnO_3$ was estimated as 54 nm at 1100 °C. The morphologies of $LaMnO_3$ nanoparticles were studied by SEM. As can be seen from Figure 1(C), $LaMnO_3$ crystal is made from spherical particles with average size of 56 nm. The purity of the nanocrystalline product was evaluated by EDX (Figure 1(D)), which showed that the sample was merely composed of La and Mn.

Characterization of GO and GO-$LaMnO_3$ nanocomposite

TEM image shown in Figure 2A proves the formation of very thin GO. The flake-like GO shows a very stable nature under irradiation of electron beam. Very thin and featureless sections are likely to be few layers of GO, suggesting that the electrochemical method is slight, but strong enough to break down the van der Waals interaction and make GO layers by fractional exfoliation of the graphite surface. As expected, TEM image of GO-$LaMnO_3$ presented in Figure 2B shows well dispersed combinations of $LaMnO_3$ nanoparticles on GO when $LaMnO_3$ and GO are mixed together, which may cause many conducting channels between the electrode and electrolyte for electron transfer.

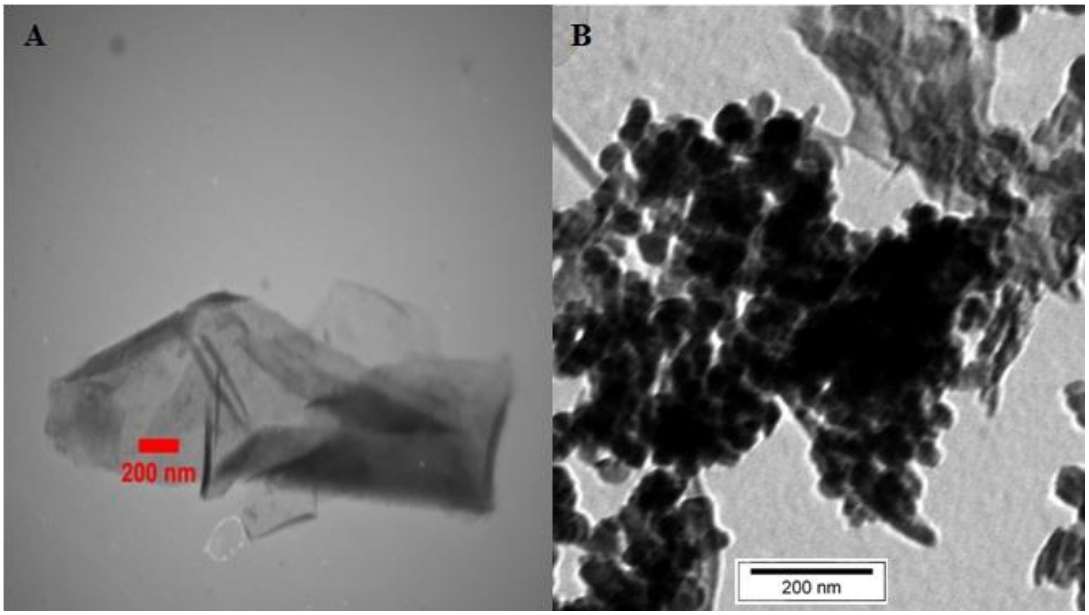

Figure 2. *TEM image of (A) GO and (B) GO-$LaMnO_3$.*

Voltammetric behavior of mixed HQ and CT

Electrochemical behavior of mixed components of HQ and CT (166.0 µM of each) in 0.1 M PBS of pH 5 was carefully investigated at the surfaces of bare GCE (BGCE), GCE/$LaMnO_3$ and GCE/GO-$LaMnO_3$ using cyclic voltammetry. BGCE electrode showed a weak and broad oxidation peak for a mixture of HQ and CT at 0.33 V (curve a in Figure 3) suggesting slow electron transfer kinetics. The

oxidation peaks of HQ and CT are merged with a very low peak current. In contrast, the GCE/$LaMnO_3$ modified electrode showed two well-defined and sharp oxidation peaks for HQ and CT at 0.11 and 0.21 V *vs.* SCE, and two corresponding reduction peaks. It can be seen from curve b in Figure 3 that the oxidation peak current for HQ and CT at GCE/$LaMnO_3$ is several times larger than that of the unmodified electrode (BGCE) because of catalytic property of $LaMnO_3$ that acts as a promoter by increasing the rate of electron transfer. The potential values of peaks shifted to less positive potentials comparing with BGCE. After addition of GO to the modifier composition, peak current values increased (curve c in Figure 3) due to high surface area and conductivity of GO. The separation of oxidation peak potential of HQ-CT was 0.1 V which is high enough for the simultaneous determination of two isomers.

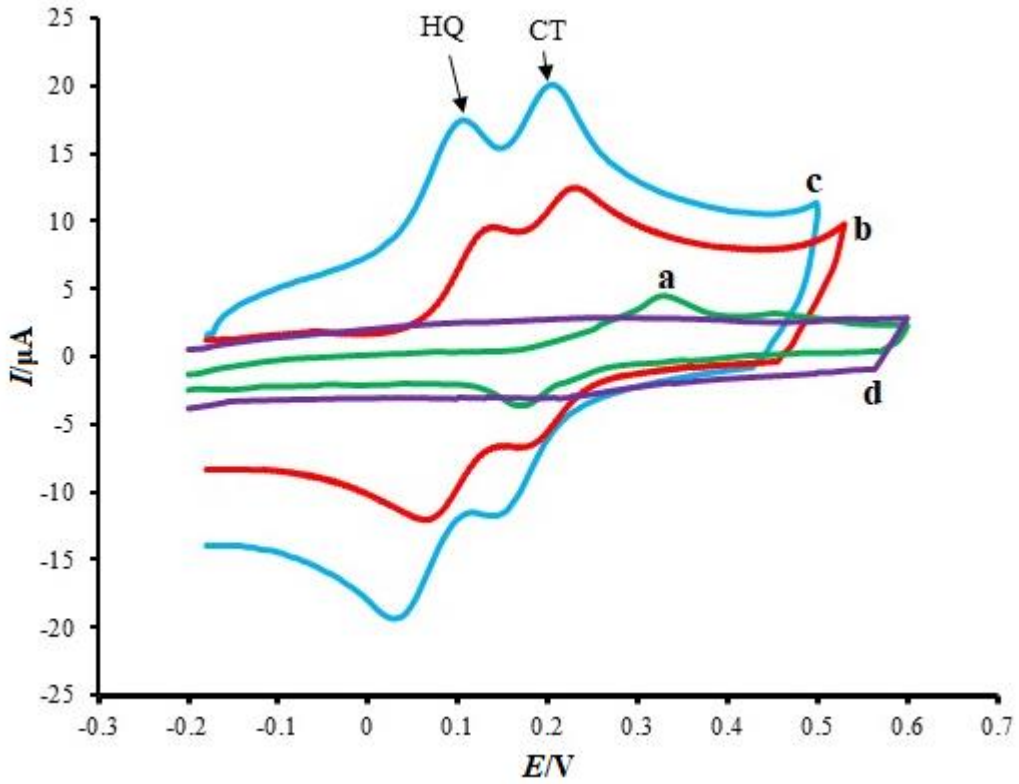

Figure 3. *CVs recorded in PBS (0.1 M pH 5) in presence of HQ and CT (166.0 µM each) at (a) BGCE, (b) GCE/$LaMnO_3$, (c) GCE/GO-$LaMnO_3$ electrodes and in absence of HQ and CT (d). Scan rate: 100 mV s^{-1}.*

Effect of pH on the oxidation of HQ and CT

The acidity of electrolyte has a significant influence on the HQ and CT electro-oxidation because protons take part in the electrode reaction. The effect of pH on GCE/GO-$LaMnO_3$ current signal was carefully investigated by cyclic voltammetry using 0.1 M buffer solutions at pH ranging from 2 to 6. The results are shown in Figure 4(A). Obviously, the peak current values of HQ and CT increased with an increase of the solution pH until pH reached 5 and then decreased. It can be seen from Figure 4(B) that the highest peak current value is for both compounds obtained at pH 5. Also, as pH of the medium was gradually increased, peak potentials for the oxidation of HQ and CT are shifted towards less positive values, showing that protons have taken part in the electrode processes. Since phosphate buffer solution at pH 5 gave the best response in terms of peak current value, peak shape and negative shift, it was selected as the optimal pH for further studies. Plot of E_p *vs.* pH for HQ and CT in the working pH range is shown in Figure 4(C). E_p values of two compounds showed linear relationship with pH of the buffer solution according to the following equations:

CT: E_p / V = −0.06 pH + 0.506 (R^2= 0.999) (1)

HQ: E_p / V = −0.063 pH + 0.41 (R^2= 0.9963) (2)

The observed slopes of 0.063 and 0.06 mV/pH for HQ and CT are close to the anticipated Nernstian value for two-electron, two-proton electrochemical reaction [46]. Therefore, it can be concluded that equal number of electrons and protons are involved in both electrode reactions. The presumed HQ and CT oxidation mechanisms are presented in Scheme 1.

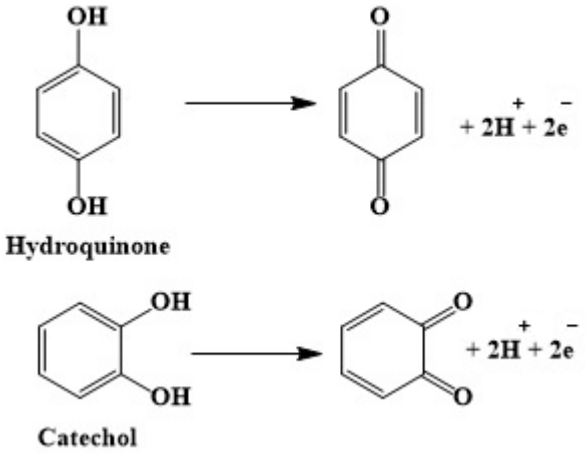

Scheme 1. Probable oxidation mechanism for HQ and CT

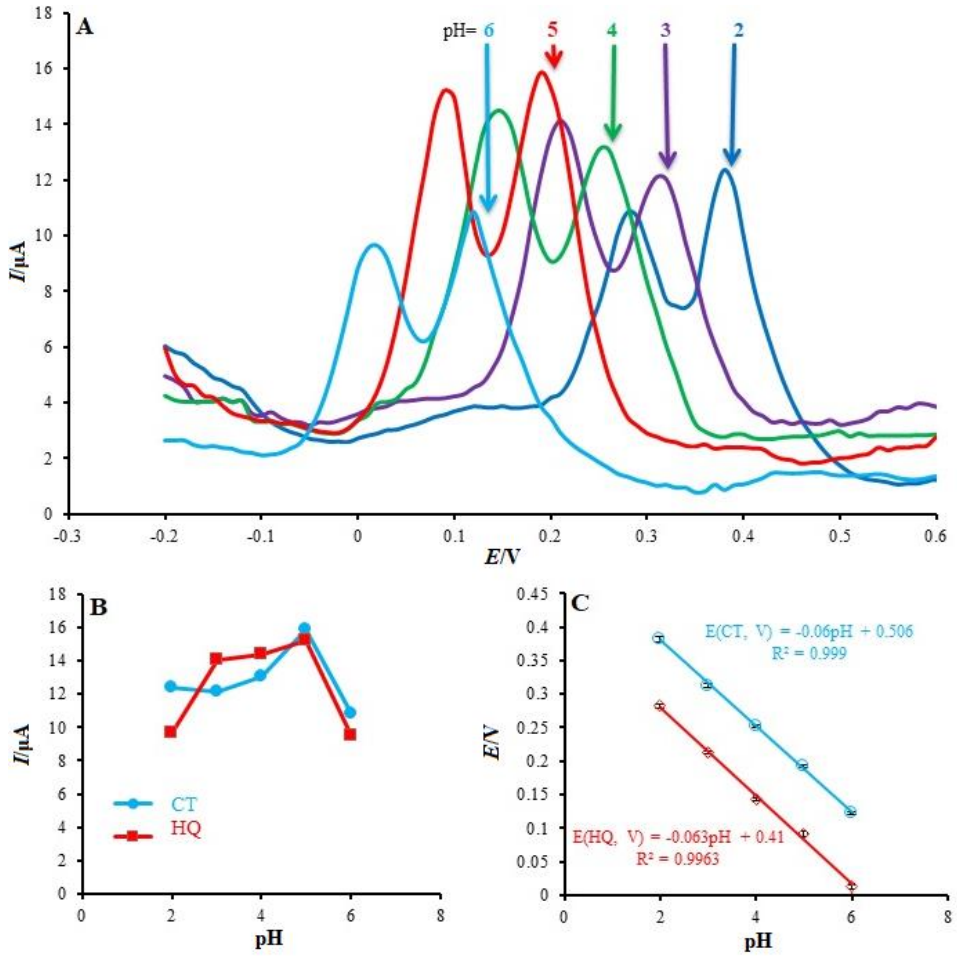

Figure 4. *(A) Effect of pH on the peak separation and peak current for the oxidation of HQ and CT (100.0 μM each); pH 2–6. Scan rate: 100 mVs^{-1}. (B) Plots of peak currents vs. pH. (C) Plots of peak potentials vs. pH.*

Influence of scan rate on electrochemical behavior of HQ and CT

The influence of the scan rate on the oxidation peak currents of HQ and CT was investigated on the GO-$LaMnO_3$ modified GCE by cyclic voltammetry. As can be seen in Figure 5(A), the peak current values continuously increase with the increase of scan rate. As shown in Figure 5(B), the current is directly proportional to the square root of the scan rate in the range of 10–1000 mV s^{-1}, which powerfully proposed that the redox reactions of HQ and CT are diffusion controlled. Also, the results show clearly that the peak separation of HQ and CT is satisfactory for their separate analysis at higher scan rates. It is additionally observed in Figure 5 that with increasing of the scan rate, potential of the oxidation peak shifted positively, while potential of the reduction peak shifted negatively. This pointed to a kinetic limitation existing at higher scan rates in the course of the reaction between the GCE/GO-$LaMnO_3$ composite and HQ and CT. Due to our study, the scan rate of 100 mV s^{-1} has to be ultimately chosen to reach the best efficiency for peak currents and peak separation.

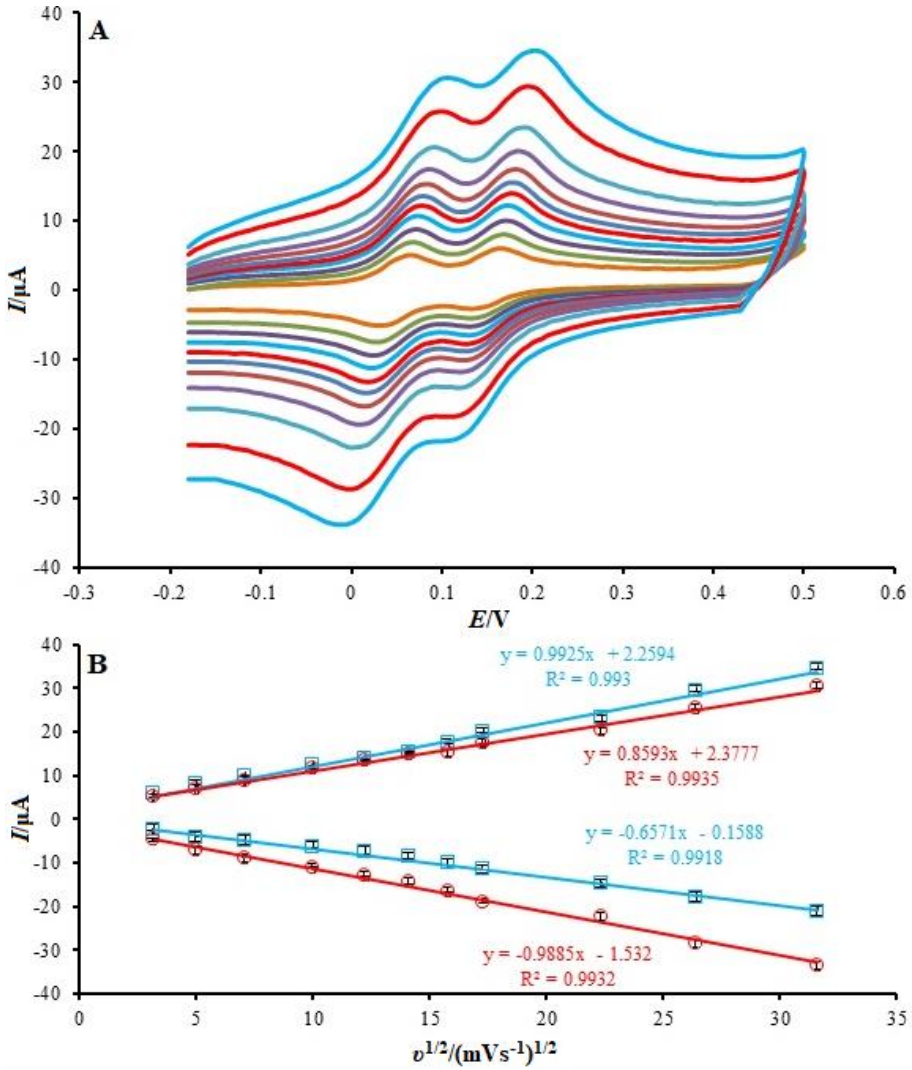

Figure 5. *(A) CVs of GCE/GO-$LaMnO_3$ electrode in pH 5 in the presence of HQ and CT (100.0 µM of each) at various scan rates (from inner to outer curve): 10, 25, 50, 100, 150, 200, 250, 300, 500, 700 and 1000 mV s^{-1}. (B) Plots of oxidation and reduction peak currents vs. $\upsilon^{1/2}$.*

Interference studies

As dihydroxybenzene isomers usually coexist in real samples, it is very important to study the interference of each other for the selective detection of the single one species. In each experiment, the concentration of one species was changed, while the concentration of the other one was kept

constant. The results are shown in Figure 6. It can be seen from Figure 6(A) that the oxidation peak current of HQ increased with an increase in the concentration of HQ, while the peak current for the oxidation of CT remained constant. The same is seen in Figure 6(C) for the voltammetric peak corresponding to the oxidation of CT. This peak increased linearly with the increase of CT concentration, whereas the peak current for the oxidation of HQ remained constant. The results presented in Figure 6 (B and D) show that peak currents are linearly proportional to the concentration of HQ and CT, respectively. The fact that by changing concentration of one species, the peak current value of the other species did not change, indicates that oxidations of HQ and CT at GO-$LaMnO_3$ modified GCE take place independently.

Interference of some other species on determination of HQ and CT was investigated by the addition of interfering species (foreign compounds) into a solution containing 40.0 µM of HQ and CT and the effects on the electrode recovery are shown in Table 1. It is clear that all kinds and amounts of interfering species (expressed as ratios between foreign compounds and HQ and CT) did not cause effects on currents being higher than ±5 %.

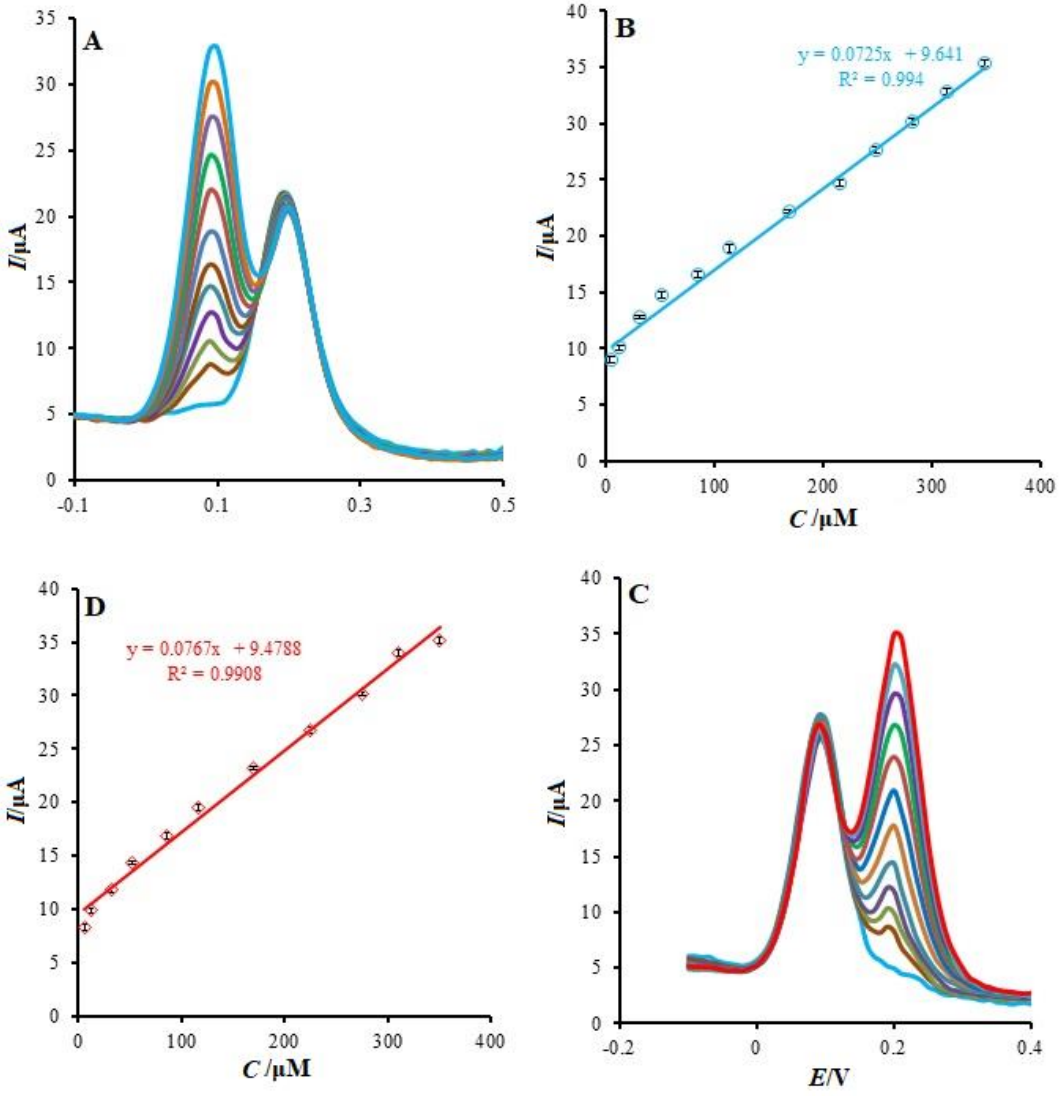

Figure 6. *DPV at the GCE/GO–$LaMnO_3$ electrode in PBS (0.1 M pH 5) (A) containing CT (166.6 µM) and different concentrations of HQ (from inner to outer): 0.0, 6.6, 13.3, 33.3, 53.3, 86.6, 116.0, 170.0, 216.6, 250.0, 283.3, 316.0 and 350.0 µM. (C) HQ (233.3 µM) and different concentrations of CT (from inner to outer): 0.0, 6.6, 13.3, 33.3, 53.3, 86.6, 116.0, 170.0, 225.0, 275.0, 310.0 and 350.0 µM. Plots of peak current vs. concentration of (B) HQ and (D) CT.*

Table 1. *Effect of interferences on determination of HQ (40.0 µM) and CT (40.0 µM).*

Foreign compound	Molar ratio of foreign compound/HQ and CT	Recovery, %
K^+ (12 mM)	300.0	98.2
Ca^{2+} (8 mM)	200.0	97.3
Zn^{2+} (12 mM)	300.0	96.0
Fe^{2+} (10 mM)	250.0	98.0
Cl^- (12 mM)	300.0	99.4
NO_3^- (16 mM)	400.0	98.0
Ascorbic acid (8 mM)	200.0	95.7
Urea (12 mM)	300.0	96.9

Simultaneous determination of HQ and CT

Differential pulse voltammetry (DPV) was performed to investigate the relationship between the peak current value and concentration of HQ and CT. As shown in Figure 7, DPV curves showed two well distinguished oxidation peaks. Electrocatalytic peak currents of HQ and CT oxidation at the surface of GCE/GO-$LaMnO_3$ are linearly dependent on HQ and CT concentrations over the range of 0.5–433.3 and 0.5–460.0 µM, respectively. Detection limit was obtained 0.06 and 0.05 µM for HQ and CT, respectively. For 7 successive determinations of 100.0 µM of HQ and CT, the relative standard deviations were 2.2 % and 1.9 %, respectively. These results show that the proposed electrode can be used effectively for the simultaneous determination of HQ and CT. Comparison of here obtained results using GCE/GO-$LaMnO_3$ electrode with the results obtained using other modified electrodes is presented in Table 2.

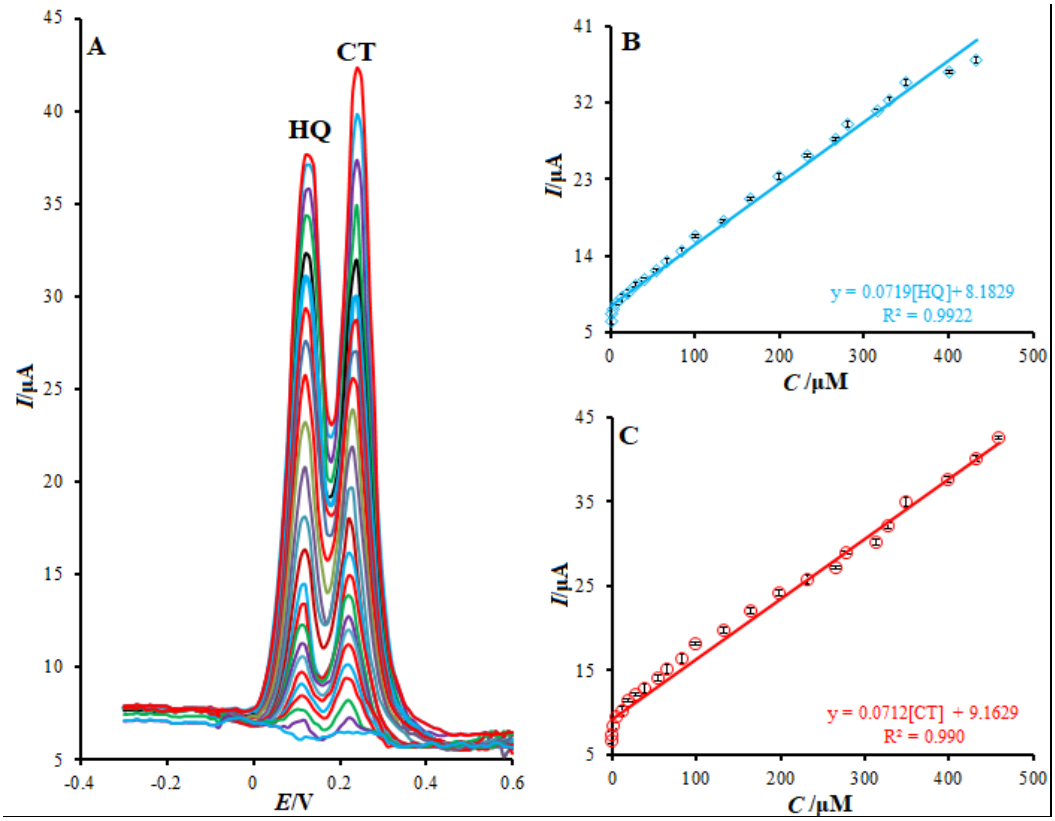

Figure 7. *(A) DPV of the mixtures of HQ and CT at the GCE/GO–$LaMnO_3$ electrode in PBS (0.1 M pH 5) at the scan rate of 100 mV s^{-1}. Concentrations from inner to outer of curves: (0.0, 0.5, 1.5, 2.0, 3.0, 6.6, 13.3, 20.0, 30.0, 40.0, 55.0, 66.6, 85.0, 100.0, 133.3, 166.6, 200.0, 233.3, 266.6, 280.0, 316.6, 330.0, 350.0, 400.0, 433.3 and 460.0). (B) and (C): Plots of oxidation peak current vs. concentration.*

Table 2. *Performance comparison of GCE/GO-$LaMnO_3$ electrode for the simultaneous determination of HQ and CT with other modified electrodes.*

Modifier	Linear range, µM		Detection limit, µM		Ref
	HQ	CT	HQ	CT	
Pt–MnO_2	3-447	15-4481	-	-	[26]
MWNTs-P3MT[a]/GCE	0.5-150	0.5-150	0.05	0.05	[28]
Gold-Graphene	1–100	1–100	0.2	0.15	[31]
RGO[b]–MWCNT	8–391	5.5–540	2.6	1.8	[47]
Carbon nanoparticle chitosan	0.8-100	0.8-100	0.2	0.2	[48]
Imidazolium ionic liquid	1-500	1-400	0.4	0.17	[49]
Nb_2O_5	0.8-500	39.8-980	1.6	0.8	[50]
Aminated glassy carbon	5-260	5-260	0.2	0.2	[51]
Graphene oxide-$LaMnO_3$	0.5-433.3	0.5-460.0	0.06	0.05	This work

[a]Poly (3-methylthiophene); [b]Reduced graphene oxide

Real sample analysis

In order to evaluate the analytical applicability of the developed method for simultaneous determination of HQ and CT, local tap and mineral waters were tested. The amounts of HQ and CT in the tap (Kerman drinking water, Kerman, Iran) and mineral (Damavand mineral water Co., Iran) water samples were determined. The reliability of the method was checked by the analysis of the samples spiked with the known amount of HQ and CT. The results are listed in Table 3. The recoveries were 95.4–102.5 % for HQ and CT. Therefore, a capability of the proposed electrode for the simultaneous determination of HQ and CT is clearly confirmed.

Table 3. *Determination of HQ and CT in water samples using GCE/GO-$LaMnO_3$ (n = 5).*

Sample	Analyte	Amount, µM			Recovery, %
		Detected	Added	Found[a]	
Tap water[b]	HQ	ND[c]	20	19.4±0.8	97.0
			30	28.6±1.0	95.4
	CT		20	20.5±0.8	102.5
			30	29.2±1.2	97.4
Mineral water[d]	HQ	ND[c]	30	28.8±1.3	96.0
	CT	ND[c]	30	29.1±1.0	97.0

[a]Mean ± standard deviation for n = 5; [b]Kerman drinking water, Kerman, Iran; [c]Not detected; [d]Damavand mineral water Co., IRAN;

Stability of modified electrode

Long term stability of modified electrode, GCE/GO–$LaMnO_3$, was assessed for a period of three weeks, when the modified electrode was stored at atmosphere conditions. DPVs showed that there were no significant variations in regard to HQ and CT oxidation peak potential values, with the exception of a drop less than 2.8 % and 2.3 % in comparison to the primary response. The adjusted electrode oxidation antifouling capacity pertaining to HQ and CT and relevant oxidation byproducts were examined via DPV evaluation.

Conclusions

For the first time, we have demonstrated an effective approach to construct of GCE/GO-$LaMnO_3$ sensor and its application for simultaneous determination of HQ and CT. Compared with the bare GCE, a large peak-to-peak separation between CT and HQ, and the significant increase of peak

current values were observed for GCE/GO-$LaMnO_3$, which clearly demonstrated that GO-$LaMnO_3$ could be used as an efficient promoter to enhance the kinetics of the electrochemical process of HQ and CT. The optimization of the experimental conditions for differential pulse voltammetry yielded a detection limit for HQ and CT of 0.06 and 0.05 μM, respectively. These values are comparable or even better than those already described in the literature. In addition, the presented sensor was applied for the simultaneous determination of HQ and CT in water samples with satisfactory results.

Acknowledgment: *This project was supported by Islamic Azad University, Kerman branch.*

References

[1] S. L. Mu, *Biosensors and Bioelectronics* **21** (2006) 1237-1243.
[2] T. Xie, Q. Liu, Y. Shi, Q. Liu, *Journal of Chromatography A* **1109** (2006) 317-321.
[3] J. Bai, L.P. Guo, J. Ndamanisha, *Journal of Applied Electrochemistry* **39** (2009) 2497-2502.
[4] Iarc Working Group, Monographs on the Evaluation of Carcinogenic Risks to Humans, **71** (1999) 433.
[5] K. Hirakawa, S. Oikawa, Y. Hiraku, I. Hirosawa, S. Kawanishi, *Chemical Research in Toxicology* **15** (2002) 76-82.
[6] S. Dong, L. Chi, Z. Yang, P. He, Q. Wang, Y. Fang, *Journal of Separation Science* **32** (2009) 3232-3238.
[7] G. Marrubini, E. Calleri, T. Coccini, A. Castoldi, L. Manzo, *Chromatographia* **62** (2005) 25-31.
[8] A. Asan, I. Isildak, *Journal of Chromatography A* **988** (2003) 145-149.
[9] M. F. Pistonesi, M. S. D. Nezio, M. E. Centurin, M. E. Palomeque, A.G . Lista, B. S. F. Band, *Talanta* **69** (2006) 1265-1268.
[10] S. C. Moldoveanu, M. Kiser, *Journal of Chromatography A* **1141** (2007) 90-97.
[11] H. Cui, Q.L. Zhang, A. Myint, X. W. Ge, L. J. Liu, *Journal of Photochemistry and Photobiology* **181** (2006) 238-245.
[12] J. A. Garcia-Mesa, R. Mateos, J. Agric, *Food Chemistry* **55** (2007) 3863-3868.
[13] I. C. Eleotério, M. Aantonio Balbino, J. F. de Andrade, B. Ferreira, A. Aparecida Saczk, L. Luiz Okumura, A. C. Ferreira Batista, M. F. de Oliveira, *Journal of Electrochemical Science and Engineering* **8** (2018) 281-289.
[14] M. M. Foroughi, Sh. Jahani, H. Hasani Nadiki, *Sensors and Actuators B* **285** (2019) 562-570.
[15] K. Roja, P. R. Prasad, P. Sandhya, N. Y. Sreedhar, *Journal of Electrochemical Science and Engineering* **6** (2016) 253-263.
[16] H. Maaref, M. M. Foroughi, E. Sheikhhosseini, M.R. Akhgar, *Analytical and Bioanalytical Electrochemistry* **10** (2018) 1080-1092.
[17] M. M. Foroughi, M. Noroozifar, M., Khorasani-Motlagh, *Journal of the Iranian Chemical Society* **12** (2015) 1139-1147.
[18] Sh. Jahani, *Analytical and Bioanalytical Electrochemistry* **10** (2018) 739-750.
[19] M. M. Foroughi, H. Beitollahi, S. Tajik, M. Hamzavi, H. Parvan, *International Journal of Electrochemical Science* **9** (2014) 2955-2965.
[20] H. Yaghoubian, Sh. Jahani, H. Beitollahi, S. Tajik, R. Hosseinzadeh, P. Biparva, *Journal of Electrochemical Science and Technology* **9** (2018) 109-117.
[21] M. Rajaei, M.M. Foroughi, Sh. Jahani, M. Shahidi Zandi, H. Hassani Nadiki, *Journal of Molecular Liquids* **284** (2019) 462-472.
[22] M. Baniasadi, Sh. Jahani, H. Maaref, R. Alizadeh, *Analytical and Bioanalytical Electrochemistry* **9** (2017) 718-728.
[23] M. Salajegheh, M. Ansari, M.M. Foroghi, M. Kazemipour, *Journal of Pharmaceutical and Biomedical Analysis* **162** (2019) 215-224.
[24] R. Torkzadeh-Mahani, M.M. Foroughi, Sh. Jahani, M. Kazemipour, H. Hassani Nadiki, *Ultrasonic Sonochemistry* **56** (2019) 183-192.
[25] J. G. Redepenning, *TrAC Trends* in *Analytical Chemistry* **6** (1987) 18-22.
[26] S. Feng, Y. Zhang, Y. Zhong, Y. Li, S. Li, *Journal of Electroanalytical Chemistry* **733** (2014) 1-5.
[27] B. Unnikrishnan, P.Ru, S. Chen, *Sensors and Actuators B* **169** (2012) 235-242.
[28] H. Zhang, J. Zhao, H. Liu, R. Liu, H. Wang, J. Liu, *Microchimica Acta* **169** (2010) 277-282.

[29] L. Wang, P. Huang, J. Bai, H. Wang, L. Zhang, Y. Zhao, *Microchimica Acta* **158** (2007) 151-157.
[30] M. Li, F. Ni, Y. Wang, S. Xu, D. Zhang, S. Chen, L. Wang, *Electroanalysis* **21** (2009) 1521-1526.
[31] X. Ma, Z. Liu, C. Qiu, T. Chen, H. Ma, *Microchimica Acta* **180** (2013) 461-468.
[32] Y. Ma, Y. Tang, K. Yin, S. Luo, C. Liu, T. Liu, L. Yang, *Journal of Electrochemical Science and Engineering* **7** (2017) 201-212.
[33] C. Z. Zhu, L. Han, P. Hu, S. J. Dong, *Nanoscale* **4** (2012) 1641-1646.
[34] K. Roja, P. Reddy Prasad, P. Sandhya, N. Yugandhar Sreedhar, *Journal of Electrochemical Science and Engineering* **6** (2016) 253-263.
[35] R. Li, T. Yang, Z. Li, Z. Gu, G. Wang, J. Liu, *Analytica Chimica Acta* **954** (2017) 43-51.
[36] F. Y. Li, J. J. Zhao, Z. F. Chen, *Journal of Physical Chemistry C* **116** (2012) 2507-2514.
[37] C. Nethravathi, M. Rajamathi, N. Ravishankar, L. Basit, C. Felser, *Carbon* 48 (2010) 4343-4350.
[38] X. Q. Yin, T. S. Jiang, Q. Zhao, H. B. Yin, *Journal of Materials Science* **47** (2012) 1026-1032.
[39] D. M. Smyth, *Ferroelectrics* **380** (2009) 1-13.
[40] F. Lichtenberg, A. Herrnberger, K. Wiedenmann, *Journal of Solid State Chemistry* **36** (2008) 253-387.
[41] P. K. Panda, *Journal of Materials Science* **44** (2009) 5049-5062.
[42] A. Dutta, T. Ishihara, H. Nishiguchi, *Chemistry of Materials* **16** (2004) 5198-5204.
[43] A. Orera, P.R. Slater, *Chemistry of Materials* **22** (2010) 675-690.
[44] Y. Yang, Y.B. Sun, Y.S. Jiang, *Materials Chemistry and Physics* **96** (2006) 234-239.
[45] M. Khorasani-Motlagh, M. Noroozifar, Sh. Jahani, *Synthesis and Reactivity in Inorganic and Metal-Organic Chemistry* **45** (2015) 1591-1595.
[46] A. J. Bard, L. R. Faulkner, *Electrochemical Methods: Fundamentals and Applications*, second ed., Wiley, New York, (2001).
[47] F. Hu, S. Chen, C. Wang, R. Yuan, D. Yuan, *Analytica Chimica Acta* **724** (2012) 40-46.
[48] M. Amiri, S. Ghaffari, A. Bezaatpour, F. Marken, *Sensors and Actuators B* **162** (2012) 194-200.
[49] X. Feng, W. Gao, S. Zhou, H. Shi, H. Huang, W. Song, *Analytica Chimica Acta* **805** (2013) 36-44.
[50] T. C. Canevari, L. T. Arenas, R. Landers, R. Custodio, Y. Gushikem, *Analyst* **138** (2013) 315-324.
[51] X. Wang, M. Xi, M. Guo, F. Sheng, G. Xiao, S. Wu, S. Uchiyama, H. Matsuura, *Analyst* **141** (2016) 1077-1082.